Journal of Atmospheric and Solar-Terrestrial Physics 105–106 (2013) 30–38

Contents lists available at ScienceDirect

Journal of Atmospheric and Solar-Terrestrial Physics

journal homepage: www.elsevier.com/locate/jastp

Seasonal variation of wave activities near the mesopause region observed at King Sejong Station (62.22°S, 58.78°W), Antarctica

Changsup Lee [a,b], Yong Ha Kim [a,*], Jeong-Han Kim [b], Geonhwa Jee [b], Young-In Won [c], Dong L. Wu [d]

[a] Department of Astronomy and Space Science, Chungnam National University, 99 Daehak-ro (St), Yuseong-gu, Daejeon 305-764, Republic of Korea
[b] Korea Polar Research Institute, 26, Songdomirae-ro (St), Yeonsu-gu, Incheon 406-840, Republic of Korea
[c] Wyle IS/National Space Science Data Center, NASA Goddard Space Flight Center, Greenbelt, MD 20771, USA
[d] NASA Goddard Space Flight Center, Greenbelt, MD 20771, USA

ARTICLE INFO

Article history:
Received 4 February 2013
Received in revised form
15 July 2013
Accepted 18 July 2013
Available online 30 July 2013

Keywords:
Gravity wave
Tide
Antarctic vortex
Neutral winds
Meteor radar

ABSTRACT

We analyzed the neutral wind data at altitudes of 80–100 km obtained from a VHF meteor radar at King Sejong Station (KSS, **62.22°S**, **58.78°W**), a key location to study wave activities above the stratospheric vortex near the Antarctic Peninsula. The seasonal behavior of the semidiurnal tides is generally consistent with the prediction of Global Scale Wave Model (GSWM02) except in the altitude region above ~96 km. Gravity wave (GW) activities inferred from the neutral wind variances show a seasonal variation very similar to the semidiurnal tide amplitudes, suggesting a strong interaction between gravity waves and the tide. Despite the consistent seasonal variations of the GW wind variances observed at the adjacent Rothera station, the magnitudes of the wind variance obtained at KSS are much larger than those at Rothera, especially during May–September. The enhanced GW activity at KSS is also observed by Aura Microwave Limb Sounder (MLS) from space in its temperature variance. The observed large wind variances at KSS imply that the Antarctic vortex in the stratosphere may act as an effective filter and source for the GWs in the upper atmosphere.

1. Introduction

Gravity waves (GW) and tides are ubiquitous in the Earth's atmosphere and very important factors in determining the dynamics and energetics of the mesospheric and lower thermospheric (MLT) region (Holton, 1983; Fritts and Alexander, 2003). They mostly originate from the lower atmosphere and propagate upward, hence efficiently transfer energy and momentum to the upper atmosphere, especially to the MLT region. GWs and tides have been studied extensively over several decades because of their significant impacts on the global atmospheric circulation and temperature structure in the upper atmosphere. While satellite observations made it possible to carry out the global structures of GW activity in the stratosphere (e.g., Wu and Jiang, 2002; Alexander et al., 2008; Wu and Eckermann, 2008), the climatology on GW activities in the local MLT region have long been studied by traditional ground-based observations such as radars (e.g., Dowdy et al., 2007; Hibbins et al., 2007; Beldon and Mitchell, 2009; Placke et al., 2010), lidars (e.g., Gardner and Liu, 2007) and optical instruments (e.g., Taylor et al., 1993; Gavrilov et al., 2002; Cho et al., 2010; Kim et al., 2010b).

In particular, meteor radars have been extensively utilized for studies of a wide range of wave spectrum from high frequency GWs to planetary waves since they can provide neutral winds and temperature data with good temporal coverage but with minimum maintenance effort: a meteor radar system is relatively simple and runs 24 h per day regardless of the weather conditions with a low power consumption. The meteor radar measurements of neutral winds and temperature near the mesopause region are also of great importance in complementing and validating satellite observations because it is difficult to probe from other techniques/sensors. Kumar and Hocking (2010) studied mean winds and tides in mesosphere using meteor radars at two different locations in the Arctic region. Recently, Beldon and Mitchell (2009, 2010) reported GW activities from meteor radar data with a simple technique and presented observational evidences for GW–tidal interactions at Rothera station (68°S, 68°W), Antarctica. The technique used in their study is appropriate for probing high frequency GWs with horizontal wavelengths of up to about 400 km, which can transfer considerable amounts of momentum to the upper atmosphere as they penetrate through high altitude regions.

King Sejong Station (hereafter KSS, 62.22°S, 58.78°W), located near the tip of Antarctic Peninsula, is often exposed to the boundary of the Antarctic winter stratospheric vortex where a great deal of GW activities occur (Baumgaertner and McDonald, 2007;

* Corresponding author. Tel.: +82 428215467; fax: +82 428218891.
E-mail address: yhkim@cnu.ac.kr (Y.H. Kim).

1364-6826/$ - see front matter © 2013 Published by Elsevier Ltd.
http://dx.doi.org/10.1016/j.jastp.2013.07.006

Vincent et al., 2007). There have been a number of studies on the upper atmospheric phenomena such as Polar Mesospheric Summer Echo (PMSE) and Polar Stratospheric Cloud (PSC) in this unique region (Höpfner et al., 2006), but the efforts have been limited to the studies on climatology of GW and tidal activities. Here, we utilize the new neutral wind measurements from the meteor radar installed at KSS to better characterize the wave activities above the Antarctic vortex boundary. This paper presents some characteristics of the mean neutral winds in the MLT region as well as wave activities (GWs and tides) derived from the wind variability.

2. Meteor radar observations

As a meteor enters the Earth's upper atmosphere, it ablates due to friction with atmospheric particles and produces a plasma trail that contains an abundance of free electrons. These free electrons within the trail can produce the backscatter of a radar signal propagating perpendicular to the trail. By observing this backscattered meteor echo, one can measure meteor decay time, radial drift velocity, and the spatial information of meteor (e.g., range and angle of arrivals). At KSS Antarctica, a VHF meteor radar has been operating since its installation on March 2007 for the purpose of studying the upper atmospheric dynamics and temperature structure near the mesopause region (e.g., Kim et al., 2010a, 2012). The KSS radar consists of 1 transmitter, 5 receivers, data acquisition systems, and radar control/analysis software. The KSS meteor radar is similar to the radar system at Davis Station, Antarctica, in terms of the operating parameters and antenna configuration: it operates at 33.2 MHz, using a solid state transmitter with a peak power of 8 kW and a maximum duty cycle of 8.4%. The operational parameters of the KSS meteor radar are summarized in Table 1. Details about the meteor radars have been described in Holdsworth et al. (2004, 2008), including the analysis technique such as 16 criteria for selecting reliable echoes.

The KSS meteor radar detects about 15,000–28,000 meteors per day, which varies with season as well as with local time. Radar data used in this study span a period of March 2007 to July 2009. In order to investigate seasonal features of neutral winds and wave activities, we only include the months with more than 15 effective observational days during the observation period. Numbers of operating days each month are listed in Table 2. Numbers in boldface indicate the number of days used in our analysis. Meteor echo data collected in March 2007 and August 2009 are excluded despite sufficient numbers of observing days since they were corrupted by software and hardware problems, respectively, resulting in uncertain spatial information.

Table 1
Operating parameters of the King Sejong meteor radar.

Parameter	Value
Frequency (MHz)	33.2
Frequency agility (kHz)	±100
Transmit power (kW)	8
Transmit polarization	Circular
EPW (m/μs)	7200/47.95
PRF (Hz)	440
Duty cycle (%)	8.4%
Receiver-filter width (kHz)	18.1
Pulse code type	4-bit complementary
Pulse shape	Gaussian
Range (km)	80–307
Range sampling resolution (km)	1.8
Coherent integrations	4
Effective sampling time (s)	0.009
Number of samples	12650
Acquisition length (s)	115

Table 2
Total observation days of meteor radar at King Sejong Station.

	Jan.	Feb.	Mar.	Apr.	May	Jun.	Jul.	Aug.	Sep.	Oct.	Nov.	Dec.
2007			31	**30**	**31**	3	–	–	–	–	**25**	**31**
2008	10	–	–	–	8	6	13	**31**	**29**	**28**	**28**	**17**
2009	**18**	**28**	**31**	**30**	**31**	**30**	**31**	31				

Numbers in boldface represent numbers of days used in the analysis.

3. Data analysis

3.1. Analysis of meteor radar data

The horizontal winds are determined from radial velocities of meteor echoes within a height–time sector of 2 km and 1 h from 78 km to 100 km. The radial velocity is determined from at least six echoes in each height–time sector by using the least squares method and the meteor echoes used for this analysis were selected only when the absolute difference between observed and projected radial velocities is less than 25 ms^{-1} (Holdsworth et al., 2004). However, these height–time averaged winds represent only the large-scale atmospheric motions such as tides, planetary waves, and mean winds. For an investigation of small-scale GWs, it is required to introduce an alternative way of wind velocity estimation whose time resolution is short enough to resolve small-scale waves. Previous studies support the interpretation that small-scale variations of the neutral winds in the MLT region are mainly due to GWs with horizontal scales significantly smaller than the typical coverage of meteor radar observations (Clark et al., 1999; Mitchell and Beldon, 2009). Since the radial drift of an individual meteor echo is directly affected by horizontal components of instantaneous wind, the variance of horizontal winds from each meteor echo within an averaging period may reflect wind fluctuation induced by GWs.

The wind variance technique, which was explained in detail in Mitchell and Beldon (2009), can be applied to study the small-scale GW effects on the horizontal wind fluctuation. The difference between the hourly average winds of a height–time sector and the estimated horizontal winds from radial velocities of individual meteor echoes within the sector can be considered to be the fluctuations of horizontal winds that respond mainly to the passage of high-frequency GWs. In this study, we used a simple assumption that large-scale atmospheric motions in the meteor observation region, which is a radius of about 250 km, are homogeneous and stay constant within a relatively short time (~1 h). Therefore, the large-scale motions can be filtered out by subtracting hourly averaged wind from the horizontal wind velocity derived from individual meteor echoes. Once we removed the contribution of the large-scale motions such as mean winds and tides, the resulting variances of horizontal winds can be used as an indicator of the total GW activity within the specific height–time sector.

The all-sky interferometric meteor radar like the one at KSS collects meteor echoes over the full range of zenith angle. However, the data used in this study are limited to the range of zenith angle between 15° and 75° in order to minimize uncertainties in the data. Meteor echoes with large zenith angles are reflected from near the horizon and may experience significant atmospheric effects including water vapor, ions and electrons along the passage of signal, which may cause errors in the determination of the range. The echoes with small zenith angles, on the other hand, could cause large errors in the determination of the horizontal winds from their radial velocities. Furthermore, the echoes near the zenith suffer from azimuthal uncertainties, adding errors to the estimated direction of the horizontal winds.

The wind data contain prevailing winds and several components of tide. The tidal components can be separated from the hourly mean winds at each height by using the least square harmonic analysis of the time series,

$$u, v = u_0 v_0 + \sum_{t=1}^{3} A_i \sin\left(\frac{2\pi}{24} t_i + \varphi_i\right),$$

where u_0 and v_0 are the zonal (positive to east) and meridional (positive to north) components of the prevailing winds, respectively, and A_i and φ_i are the amplitude and phase at the time of maximum amplitude, respectively. The index i indicates diurnal ($i=1$), semidiurnal ($i=2$), and terdiurnal ($i=3$) components of tide. A four-day window was used for each time series of the hourly mean winds. The least-square fitting process was performed only if there were at least 48 h continuous data in a given window. Once the tidal parameters were determined for a specific time–height sector, the four-day window was shifted forward by 1 day and the fitting process was repeated. A vector average of tidal components was used to investigate monthly mean tidal features. The number of meteor echoes in a height–time sector is also an important statistical factor for this technique to check whether the results are reliable. A running median with 8 h-width and 4 h-shift window has been used to smooth out extreme values of wind variances in a given height time sector on a daily basis. Meteors above 100 km and below 80 km are not included since the meteor count rates in those regions are not large enough to obtain reliable wind variance. The height width of 4 km has been used to collect sufficient meteor echoes at each height sector. In order to obtain the continuous wave field, a given height sector moves upward by 2 km and shares 2 km overlapped height region with adjacent one. Wind variances are thus obtained in nine height sectors with median heights of 82–98 km.

3.2. Analysis of MLS data

In order to validate and compare with the GW activities obtained from meteor radar data at KSS we analyzed 118 GHz O_2 saturated radiance data measured by Microwave Limb Sounder (MLS) onboard the Aura satellite. The MLS limb radiances are very sensitive to the temperature fluctuation induced by GWs with short (100–200 km) horizontal wavelengths and long (>5 km) vertical wavelengths in the lower height ranges from about 20–55 km. The 25 channels are symmetrically distributed around the center line (channel 13) over wing line emissions, and a pair of channels effectively probes an atmospheric layer between 22 and 55 km. Following the technique of estimating GW activity developed by Wu and Eckermann (2008), we utilized at least 40 saturated radiance measurements at the bottom of each scan in order to guarantee a quality of the GW-induced temperature variances. Linear fitting procedure should be carried out to isolate perturbations by removing a linear trend and tangent height dependence since the radiance measurements can be affected by viewing angle of the instrument. The variance of the radiance can be derived from following equation:

$$\sigma^2 = \frac{1}{4} \sum_{t=1}^{40} (y_i - y_m)^2$$

where y_i and y_m denote, respectively, measured radiances of the channel and a linear fitting function. This function can be determined from the least square fit to the 40 measurements. The variance of radiance is mainly due to atmospheric temperature fluctuations, instrument noise and non-linear terms of the pressure variations (Wu and Waters, 1996). The GW-induced variances can be estimated by subtracting instrument noise variance (σ_e^2) and non-linear terms from the initially calculated variances. A monthly mean within a $5^\circ \times 10^\circ$ latitude–longitude region has been applied to extend the minimum detectable variance of channel 1(or 25) to 2.3×10^{-3} K^2. The uncertainty of the variance can be reduced to $023\sigma_e^2/\sqrt{N}$ when N independent variance measurements are averaged.

4. Results and discussions

4.1. Mean winds

Monthly mean winds for each month are computed from daily mean winds in whole observational period, and are presented as contour plots of Fig. 1. Monthly mean zonal winds (top panel) show dominant eastward wind over all observation heights during a whole year except summer when there exist the strongest westward winds below the mesopause. The zonal wind observed at KSS follows the typical characteristics of the wind in the southern high latitude regions; strong eastward wind appears at around 95 km and 80 km altitudes in late summer and mid winter, respectively, but there is no significant feature in autumn

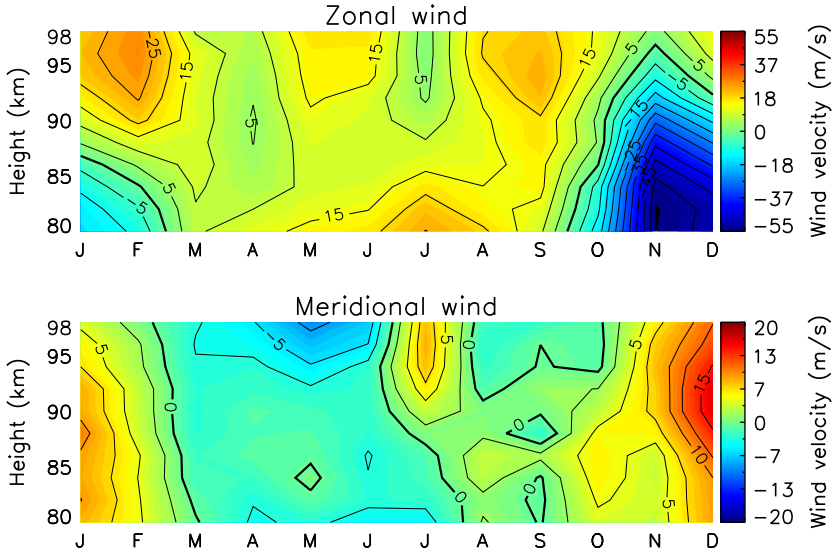

Fig. 1. Monthly mean zonal (top) and meridional (bottom) winds observed from King Sejong Station (KSS). Winds are averaged over two adjacent 2 km height sectors, and presented at the median altitude. Thick lines represent zero wind speed. Westward/southward are indicated by negative signs.

(Dowdy et al., 2007; Sandford et al., 2010). Note that the zonal wind shows the strong vertical wind shear during the period of November through February. The maximum wind shear occurs at around 90 km altitude in the early summer (November–December). As summer progresses the strong westward wind at lower altitudes below about 90 km becomes weak but at higher altitudes the weak eastward wind increases gradually up to about 30 ms^{-1} in February.

Although the meridional wind is more variable in its direction and weaker in its strength compared with the zonal wind, it also shows evident seasonal features such as equinox minima and solstice maxima (bottom panel in Fig. 1). While the weak poleward wind is dominant in autumn, the weak equatorward wind ($\sim$5 ms^{-1}) appears in spring. Relatively large equatorward wind occurs in summer at all observation heights, with the maximum reaching up to 20 ms^{-1} at 90 km in December. It is worth noting that the height of peak equatorward wind in summer coincides with the region of the maximum zonal wind shear and may be attributed to the breakdown of gravity waves. Similar coincidence has been noted in Arctic mesosphere (Mitchell et al., 2002). It has been well known that momentum deposition associated with wave dissipation near the mesopause region causes zonal wind drag, which in turn drives meridional circulation (e.g., Shepherd, 2000). In winter, however, the wind pattern seems to show large year-to-year variability in particular at the lower heights below about 90 km (not shown in figure). Note that, in their analysis of mean winds at Rothera station, Antarctica, Sandford et al. (2010) observed large year-to-year variation of the meridional wind at the upper heights (above 94 km) in winter during the periods of 2005–2009. In order to confirm this variability of the meridional wind at KSS, it is required to continue our observation to collect wind data for longer periods than the current study.

4.2. Tides

Figs. 2 and 3 show the height profiles of amplitudes (left panels) and phases (right panels) of the semidiurnal tides at KSS for the zonal and meridional components, respectively. Corresponding height profiles obtained from GSWM02 at 60°S latitude and 60°W longitude (nearest available) are also presented for comparison with the data. The measured amplitudes tend to increase with height, reach their maxima at around 96 km and reverse the growth above this height for most periods. the output from GSWM02 does not show the peak height of tidal waves; rather, the model amplitudes keep increasing with height continuously all the way up to the upper limit. In general, the observed semidiurnal amplitudes agree with the GSWM02 in their seasonal variations: the amplitudes are mostly larger in winter than in summer. However, the observed maximum amplitude occurs in May while the model shows the maximum amplitude in August. In addition, our observation shows relatively larger amplitudes than the GSWM02 for most periods. Both the zonal and meridional tidal components show all these characteristics of the amplitude in a similar fashion.

The phases in Figs. 2 and 3 are defined as the time for the zonal and meridional winds to reach their first maximum values measured in universal time. This piece of information can provide the important properties of tidal winds such as their vertical propagation. The height profiles of the phases show the evident downward progression of the phase, implying that tidal wave energy transports to the higher altitude as the semidiurnal tide propagates upward. Note that

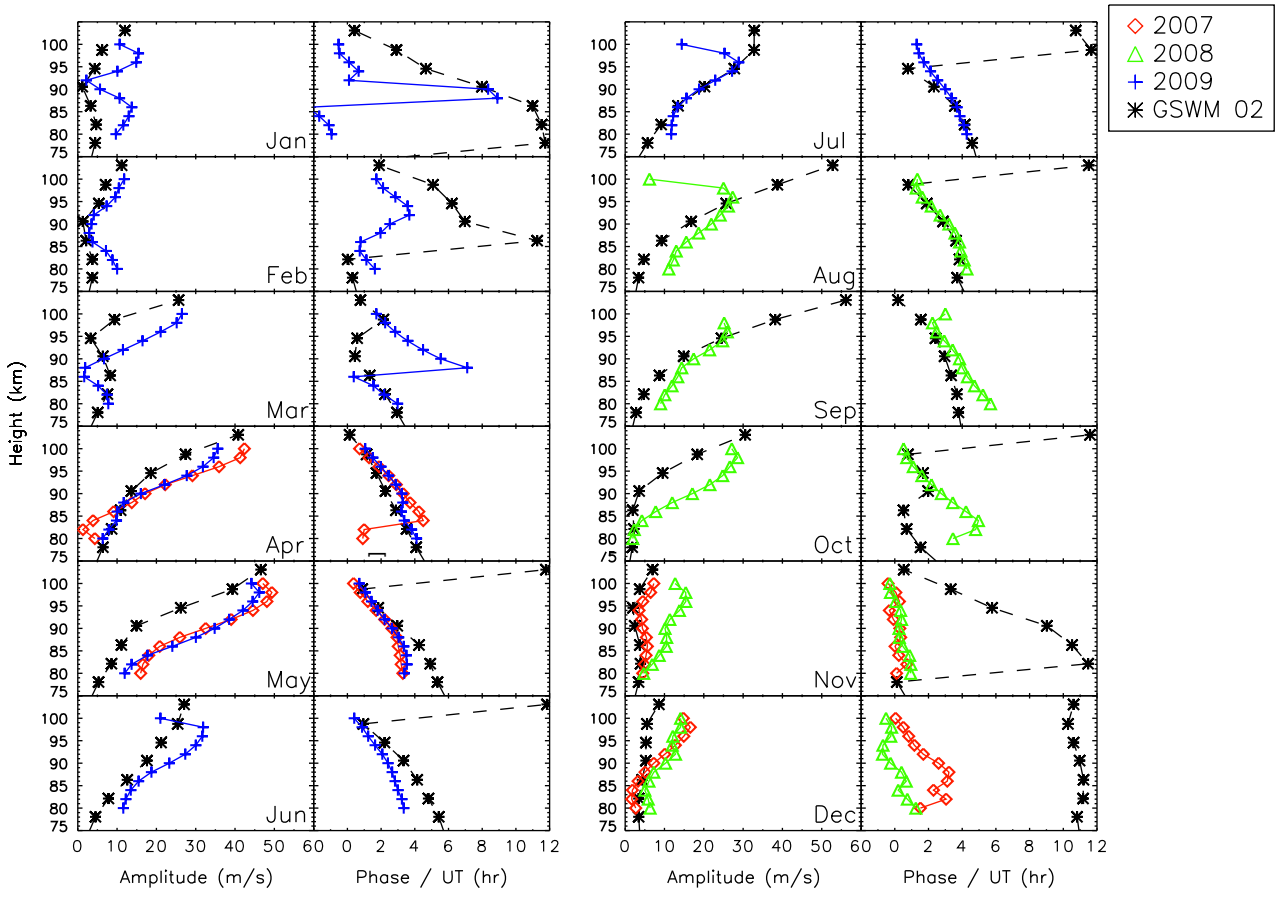

Fig. 2. Height profiles of the amplitudes and phases of the zonal component of the semidiurnal tide during all observation period. The amplitudes and phases are averaged over two adjacent 2 km height sectors, and presented at the median altitude. Data shown are for the years 2007 (diamond), 2008 (triangle), and 2009 (plus sign). GSWM02 values are also presented for comparison.

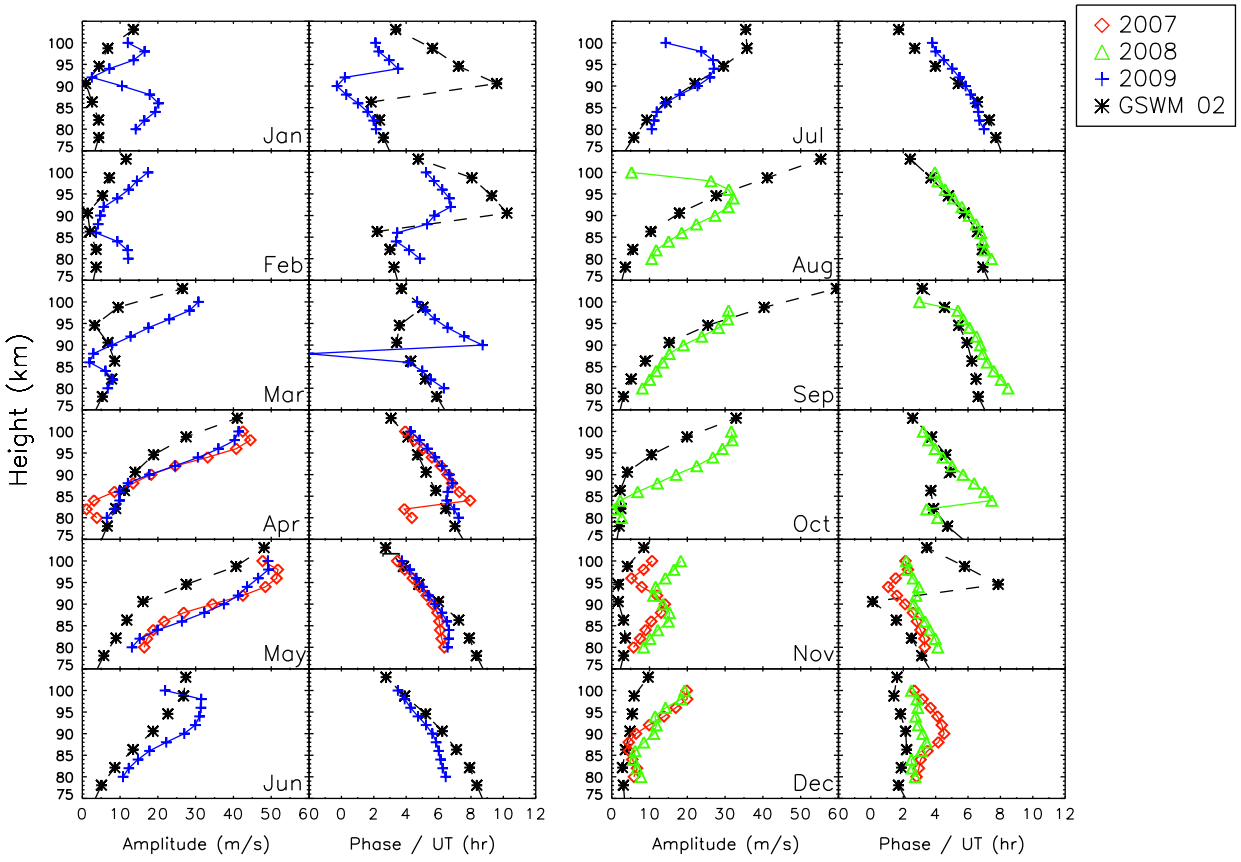

Fig. 3. Same as in Fig. 2, but for the meridional component.

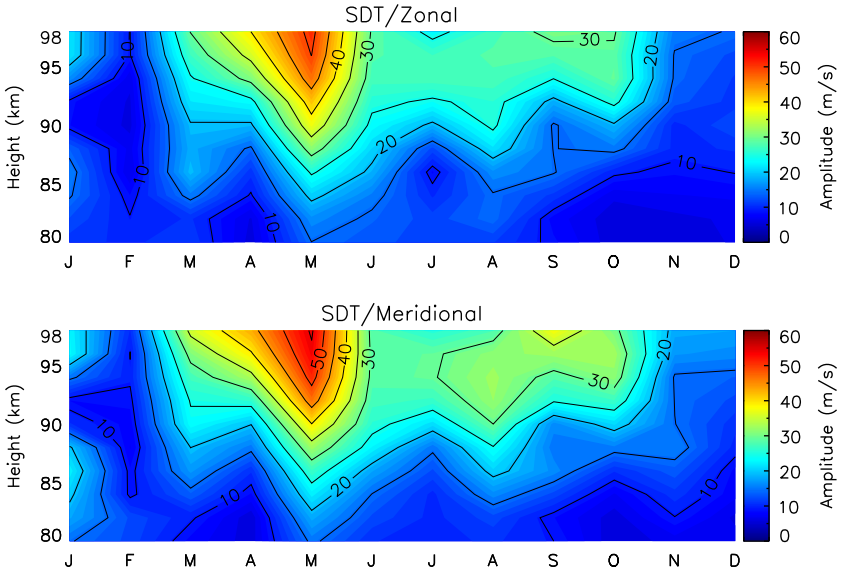

Fig. 4. Height–month contour plot of the seasonal variation of the amplitude of the zonal (upper) and meridional (lower) semidiurnal tide over King Sejong Station.

the semidiurnal tidal component shows quadrature phase: that is, the zonal component precedes the meridional component by ~3 h at all heights and in all months. This phase difference between the two components indicates that the tidal wind vector rotates anticlockwise in an approximately circularly polarized manner. The vertical wavelength of semidiurnal tides can be derived from the gradient of phase with respect to the height. The calculated vertical wavelength ranges between 50 and 90 km, except for summer (November and December) when it tends to reach infinity; that is, the phase does not change much with height during summer at KSS.

In order to further investigate the seasonal features of the semidiurnal tide, we present height–month contour plots of the monthly mean tidal amplitudes over the period of 2007–2009 in Fig. 4. The amplitudes of the zonal and meridional components are very similar to each other during the whole observation period. Maximum amplitude of the semidiurnal tide appears in around May at higher altitudes and tends to continue throughout the whole winter until the amplitudes are diminished considerably (about 20 ms^{-1} at 100 km) in November. It is noted that there is a sudden increase in the amplitude across entire height range in

March and the enhanced amplitude remains through June. The seasonal variations of semidiurnal tidal amplitude observed at KSS are consistent with results from Rothera (Beldon and Mitchell, 2010) in its magnitude and height profile except that the amplitudes at KSS are weaker at higher altitude regions (above ~94 km) in summer. In the Arctic MLT region observed by a meteor radar at Esrange, largest amplitudes of semidiurnal tide were reported both in the late summer months and in winter (Mitchell et al., 2002). Kumar and Hocking (2010) also observed tides in the Arctic region with meteor radars. Semidiurnal tidal vectors in the Arctic region, however, rotate clockwise, opposite direction to ours in the Antarctic region.

4.3. Gravity wave activity

Contour plots for monthly means of median wind variances are presented in Fig. 5. Notice that the lowest altitude of Fig. 5 is 82 km due to data lower limit of 80 km, instead of 78 km used for mean wind and tide analyses. Wind variances in Fig. 5 shows a remarkable similarity in their morphology to the monthly mean tidal amplitudes in Fig. 4 except for the enhancement of the wind variances at lower heights at the beginning of summer. For most seasons, the variances increase with height except for November and December, during which the variances decrease with height below about 90 km. A clear seasonal variation is seen in both the zonal and meridional winds with maxima at higher altitudes in May and around September. In particular, just as in the tidal amplitude in Fig. 4, the sudden and large enhancements occur in May, which may indicate that the gravity wave activity suddenly increases at lower atmosphere around in May near the KSS. It has been known that there is the formation and breakdown of Antarctic vortex in the lower atmosphere (from the upper troposphere through the stratosphere) in autumn and spring, respectively, which may partially contribute to the enhancement of GW activity (Yoshiki et al., 2004).

A direct comparison between semidiurnal tidal amplitudes and wind variances clearly shows a remarkable agreement in their seasonal variations across the entire height range. This result can be an important clue attributing the cause of the similarity to the interactions between GWs and tides. Several numerical studies have demonstrated that GWs and tides become amplified through interaction with each other (e.g., Mayr et al., 2005a, 2005b; Liu et al., 2008). There are also a number of observational evidences of tidal modulation of GWs from optical and radar measurements (e.g., Espy et al., 2004; Beldon and Mitchell, 2010). They concluded that at high latitudes the upward momentum carried by GWs is modulated by the semidiurnal tide and the resulting momentum significantly contributes to the observed variations of the semidiurnal tide.

As pointed out earlier in this section, however, the height profiles of the amplitudes of the semidiurnal tides and the wind variances show significantly different behaviors in early summer (i.e., November and December) as presented in Figs. 4 and 5, respectively. In general, GWs can propagate upward with slower phase velocities and they are strongly affected by the background wind, primarily the zonal wind, unlike tides (Smith, 2004). The strong westward wind between 80 km and 90 km altitudes during early summer (see Fig. 1) may cause the GW amplitudes to break significantly as they propagate through the background wind as seen in Fig. 5, but to reduce tidal amplitudes only to the small degree as seen in Fig. 4.

The similar height profiles of wind variances seen in our study during early summer have been reported in a number of studies by using radar observations at middle and high latitudes (e.g., Vincent and Fritts, 1987; Dowdy et al., 2007; Beldon and Mitchell, 2009; Placke et al. 2010). This behavior of wind variances in summer has been related to the corresponding background winds, especially the zonal wind. It has been known that the zonal wind has more significant seasonal variation and much larger magnitude than the meridional wind (Sandford et al., 2010). Thus the zonal wind tends to have greater effects on the propagation of GWs, which was studied in terms of the critical-level filtering by Taylor et al. (1993) and Dowdy et al. (2007). Beldon and Mitchell (2009), on the other hand, concluded that the critical-level filtering can only explain the observed wind variances below 80 km and presumed the steeper temperature gradients around the mesopause region in summer being more likely to induce GW breaking. As the GWs reach above 80 km, they may dissipate through the convective and dynamic instability of the background air. The dissipation of GWs can deposit the energy and momentum to the background atmosphere, which then results in strong deceleration of the westward wind above the 80-km altitude and eventually reverses it to eastward near 90 km. The wind variances observed at KSS show rapid decrease of the amplitude with height as shown in Fig. 5, which implies the significant dissipation of GWs in summer. It should be noted that the zonal wind also shows a very rapid decrease with height in summer (Fig. 1).

Although the seasonal and height dependences of wind variances are consistent with previous studies in different southern

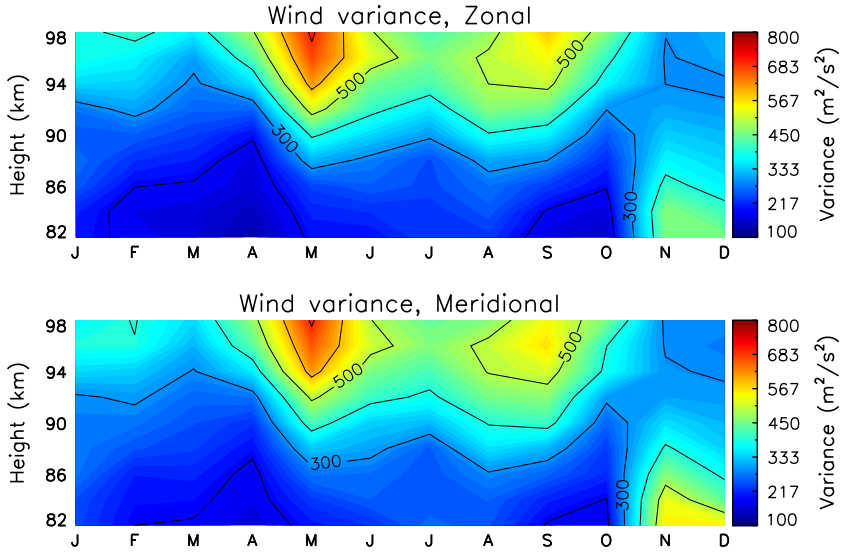

Fig. 5. Height–month contour plots of the monthly mean of median zonal (upper) and meridional (lower) wind variances.

high latitude regions, the wind variances over KSS are larger than those observed at Rothera station which is located in the middle of the Antarctic Peninsula (see Fig. 6, Mitchell and Beldon, 2009). In particular, this difference becomes significant above 88 km with a ratio as large as ~1.5 at 98 km during the winter season. These discrepancies imply that the generation and progression of GWs can be significantly affected by spatially localized sources and background environments such as local GW breakings and wind fields (Fritts et al., 2006). Whiteway et al. (1997) and Baumgaertner and McDonald (2007) reported a strong enhancement of wave energy at the boundary of the polar vortex and concluded that the large zonal winds near the polar vortex lead to the Doppler shift of the vertical wavelength of GWs with relatively small phase velocity to larger wavelength. This large vertical wavelength allows GWs to grow to larger amplitudes before they saturate and to reach the level of instability at higher altitudes where their energy and momentum are deposited to the background atmosphere.

Furthermore, from the global scale observations of GW activity in the lower atmosphere by satellites such as Challenging Minisatellite Payload (CHAMP) and Constellation Observing System for Meteorology, Ionosphere and Climate (COSMIC), it was found that the maximum values of temperature variance and momentum flux due to GW occur over the tips of the Antarctic Peninsula and South

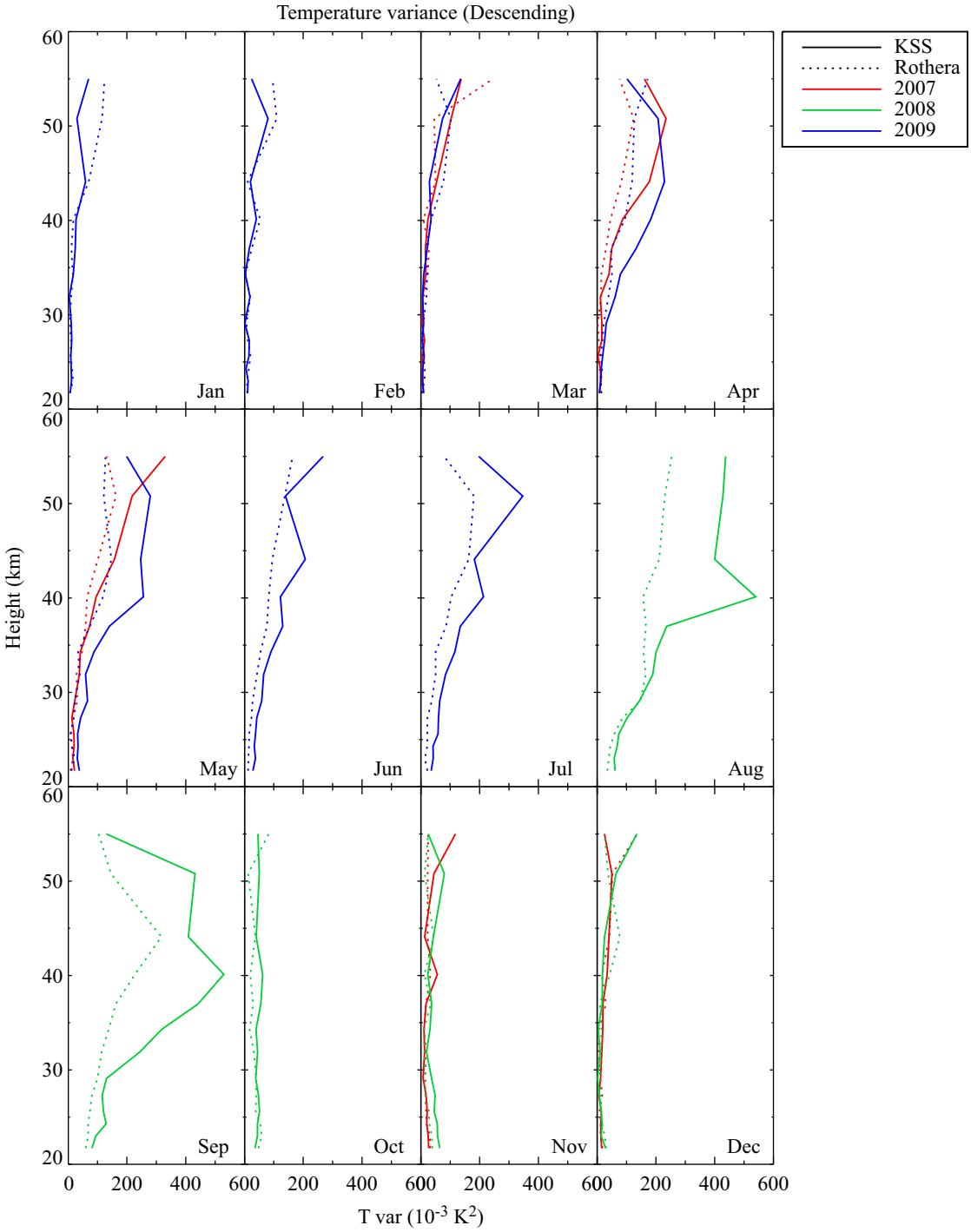

Fig. 6. Height profiles of the monthly mean descending temperature variance from Aura-MLS for 2007–2009 over KSS (solid lines) and Rothera (dotted lines).

America during winter from June through August (Baumgaertner and McDonald, 2007; Alexander et al., 2009). In addition, Duck et al. (2001) demonstrated that the zonal wind strength in the lower stratosphere is an important factor to determine wave propagation condition by showing a close link between the GW activity and geographic location relative to the vortex.

Fig. 6 shows the monthly mean temperature variances for the descending mode of the Aura satellite observation over KSS (solid lines) and Rothera (dotted lines), respectively, during the periods of KSS meteor radar observations. Since temperature variances for the ascending mode have identical features on both height profile and seasonal variation, only descending mode or nighttime data are used in this study. The amplitudes of the temperature variance generally increase with height throughout the year except in the lower stratosphere during summer (November–February). Although the seasonal dependence of temperature variance over KSS tends to be analogous to that over Rothera, there is a difference in the magnitude between two regions, being larger at KSS than at Rothera in general. This difference in temperature variances is clearly visible from April through September and the maximum difference is observed in August and September. The result is very similar to the difference in wind variances obtained from meteor radars at the two stations that becomes significant above 88 km with a maximum ratio of $\sim$1.5 at 98 km during the winter season. Gimeno et al. (2007) reported that the Antarctic vortex in the southern hemisphere is strongest during this period and the maximum zonal wind occurs at about 60°S. Since the larger wind variance at KSS implies that the GW activity is larger at KSS than at Rothera, the large temperature variances in the stratosphere over the KSS from winter to early spring may support the idea that the upward propagation of GWs is strengthened by reduced filtering effect and Doppler shift due to the large zonal wind at the boundary of the vortex during this season (Yoshiki et al., 2004). The results described above also support previous studies suggesting that stronger GW activity occurs near the edge of the Antarctic vortex in winter and spring (e.g., Jiang et al., 2002; Jiang et al., 2005; Baumgaertner and McDonald, 2007).

5. Summary and conclusions

The mesospheric wind data from the KSS VHF meteor radar were analyzed for the period of April 2007 – July 2009 to investigate the gravity wave activity in the mesopause region over KSS, Antarctica. The mean zonal wind generally shows the dominant eastward flow at 80–100 km with a large annual variation. It reverses to a westward flow during summer (November and December) at $\sim$80 km altitude, showing the strongest jet as high as -55 ms^{-1}. During summer, the westward wind shows conspicuous features such as strong vertical wind shear in the altitude region of 80–95 km and wind reversal from the westward to the eastward above the mesopause region. For the meridional winds, there is a relatively large equatorward wind at 80–100 km during summer, which can reach as large as 20 ms^{-1} at 90 km in December. Likely due to the interaction between GWs and zonal winds, the peak of equatorward winds occurs at about 90 km altitude where the zonal wind shear is strongest. The seasonal behaviors of mean winds over KSS agree well with the meteor radar observation at Rothera (a nearby station in the Antarctic peninsula).

The semidiurnal tide is found to be the strongest among all the tidal components near the mesopause region over KSS. The properties of monthly averaged semidiurnal tides are generally in good agreement with the prediction of GSWM02 except for the amplitudes at higher altitudes than 95 km. Strong semidiurnal-tidal activity occurs during March to October. There is a clear 3-h phase difference between the zonal and meridional components, implying that the tide propagates upward with a circular polarized structure at all heights and in all seasons. The seasonal variation of semidiurnal tide generally resembles that of the wind variance, which supports the inter-relationship between the tide and GWs as reported in previous observations and theoretical predictions (Fritts and Vincent, 1987; Espy et al., 2004; Mayr et al., 2005a, 2005b; Beldon and Mitchell, 2010).

The vertical profiles of the estimated wind variances show an increasing trend with height in all seasons, except for summer when the variance decreases with height especially at lower altitudes (82–90 km). The strength of wind variances at KSS is significantly larger than that in the Rothera station above the mesopause regions ($\sim$88 km) from May through September. Aura MLS satellite observations show significantly larger stratospheric temperature variances over KSS than over Rothera station during August and September. The global scale satellite observations of GW activity in the lower atmosphere, for example, from CHAMP and COSMIC satellites also indicate that the maximum temperature variance and momentum flux due to GW occur over the tips of Antarctic Peninsula and South America during winter. Therefore we conclude that the observed large wind variances at KSS are caused by the very effective atmospheric condition near the Antarctic vortex.

Acknowledgment

This work was supported by research funds PE13010 from Korea Polar Research Institute.

References

Alexander, M.J., Gille, J., Cavanaugh, C., Coffey, M., Craig, C., Eden, T., Francis, G., Halvorson, C., Hannigan, J., Khosravi, R., Kinnison, D., Lee, H., Massie, S., Nardi, B., Barnett, J., Hepplewhite, C., Lambert, A., Dean, V., 2008. Global estimates of gravity wave momentum flux from High Resolution Dynamics Limb Sounder (HIRDLS) observations. Journal of Geophysical Research 113 (D15), http://dx.doi.org/10.1029/2007JD008807.

Alexander, S.P., Klekociuk, A.R., Tsuda, T., 2009. Gravity wave and orographic wave activity observed around the Antarctic and Arctic stratospheric vortices by the COSMIC GPS-RO satellite constellation. Journal of Geophysical Research 114 (D17), http://dx.doi.org/10.1029/2009JD011851.

Baumgaertner, A.J.G., McDonald, A.J., 2007. A gravity wave climatology for Antarctica compiled from Challenging Minisatellite Payload/Global Positioning system (CHAMP/GPS) radio occultations. Journal of Geophysical Research 112 (D5), http://dx.doi.org/10.1029/2006JD007504.

Beldon, C.L., Mitchell, N.J., 2009. Gravity waves in the mesopause region observed by meteor radar, 2: Climatologies of gravity waves in the Antarctic and Arctic. Journal of Atmospheric and Solar-Terrestrial Physics 71, 875–884.

Beldon, C.L., Mitchell, N.J., 2010. Gravity wave–tidal interactions in the mesosphere and lower thermosphere over Rothera, Antarctica (68°S, 68°W). Journal of Geophysical Research 115 (D18), http://dx.doi.org/10.1029/2009JD013617.

Cho, Y.-M., Shepherd, M.G., Shepherd, G.G., 2010. Wave perturbations in the MLT at high northern latitudes in winter, observed by two SATI instruments. Advanced in Space Research 45 (1), 45–55.

Clark, R.R., Tate, R.J., Salah, J.E., Goncharenko, L.P., 1999. Common-volume measurements of mesospheric winds: 2. Small scale structure implications. Journal of Atmospheric Solar-Terrestrial Physics 61 (17), 1273–1287.

Dowdy, A.J., Vincent, R.A., Tsutsumi, M., Igarashi, K., Murayama, Y., Singer, W., Murphy, D.J., 2007. Polar mesosphere and lower thermosphere dynamics: 1. Mean wind and gravity wave climatologies. Journal of Geophysical Research 112 (D17), http://dx.doi.org/10.1029/2006JD008126.

Duck, T.J., Whiteway, J.A., Carswell, A.I., 2001. The gravity wave–arctic stratospheric vortex interaction. Journal of the Atmospheric Sciences 58, 3581–3596.

Espy, P.J., Jones, G.O.L., Swenson, G.R., Tang, J., Taylor, M.J., 2004. Tidal modulation of the gravity-wave momentum flux in the Antarctic mesosphere. Geophysical Research Letters 31 (11), http://dx.doi.org/10.1029/2004GL019624.

Fritts, D.C., Vincent, R.A., 1987. Mesospheric momentum flux studies at Adelaide Australia: observations and a gravity wave–tidal interaction model. Journal of the Atmospheric Sciences 44, 605–619.

Fritts, D.C., Alexander, M.J., 2003. Gravity wave dynamics and effects in the middle atmosphere. Reviews of Geophysics 41 (1), http://dx.doi.org/10.1029/2001RG000106.

Fritts, D.C., Vadas, S.L., Wan, K., Werne, J.A., 2006. Mean and variable forcing of the middle atmosphere by gravity waves. Journal of Atmospheric and Solar-Terrestrial Physics 68, 247–265.

Gardner, C.S., Liu, A.Z., 2007. Seasonal variations of the vertical fluxes of heat and horizontal momentum in the mesopause region at Starfire Optical Range, New

Mexico. Journal of Geophysical Research 112 (D9), http://dx.doi.org/10.1029/2005JD006179.
Gavrilov, N.M., Shiokawa, K., Ogawa, T., 2002. Seasonal variations of medium-scale gravity wave parameters in the lower thermosphere obtained from spectral airglow temperature imager observations at Shigaraki, Japan. Journal of Geophysical Research 107 (D24), http://dx.doi.org/10.1029/2001JD001469.
Gimeno, L., Torre, L., Nieto, R., Gallego, D., Ribera, P., García-Herrera, R., 2007. A new diagnostic of stratospheric polar vortices. Journal of Atmospheric and Solar-Terrestrial Physics 69 (15), 1797–1812.
Hibbins, R.E., Espy, P.J., Jarvis, M.J., Riggin, D.M., Fritts, D.C., 2007. A climatology of tides and gravity wave variance in the MLT above Rothera, Antarctica obtained by MF radar. Journal of Atmospheric and Solar-Terrestrial Physics 69 (4–5), 578–588.
Holdsworth, D.A., Reid, I.M., Cervera, M.A., 2004. Buckland Park all-sky interferometric meteor radar. Radio Science 39 (5), http://dx.doi.org/10.1029/2003RS003014.
Holdsworth, D.A., Murphy, D.J., Reid, I.M., Morris, R.J., 2008. Antarctic meteor observations using the Davis MST and meteor radars. Advances in Space Research 42 (1), 143–154.
Holton, J.R., 1983. The influence of gravity wave breaking on the general circulation of the middle atmosphere. Journal of the Atmospheric Science 40 (10), 2497–2507.
Höpfner, M., Larsen, N., Spang, R., Luo, B.P., Ma, J., Svendsen, S.H., Eckermann, S.D., Knudsen, B., Massoli, P., Cairo, F., Stiller, G., Clarmann, T.V., Fischer, H., 2006. MIPAS detects Antarctic stratospheric belt of NAT PSCs caused by mountain waves. Atmospheric Chemistry and Physics 6 (5), 1221–1230.
Jiang, J.H., Wu, D.L., Eckermann, S.D., 2002. Upper Atmosphere Research Satellite (UARS) MLS observation of mountain waves over the Andes. Journal of Geophysical Research 107 (D20), http://dx.doi.org/10.1029/2002JD002091.
Jiang, J.H., Eckermann, S.D., Wu, D.L., Hocke, K., Wang, B., Ma, J., Zhang, Y., 2005. Seasonal variation of gravity wave sources from satellite observation. Advances in Space Research 35 (11), 1925–1932.
Kim, J.-H., Kim, Y.H., Lee, C.S., Jee, G., 2012. Mesospheric temperature estimation from meteor decay times of weak and strong meteor trails. Journal of Atmospheric and Solar-Terrestrial Physics 89, 18–26.
Kim, J.-H., Kim, Y.H., Lee, C.-S., Jee, G., 2010a. Seasonal variation of meteor decay times observed at King Sejong Station (62.22°S, 58.78°W), Antarctica. Journal of Atmospheric and Solar-Terrestrial Physics 72 (11–12), 883–889.
Kim, Y.H., Lee, C.S., Chung, J.-K., Kim, J.-H., Chun, H.-Y., 2010b. Seasonal variations of Mesospheric gravity waves observed with an airglow all-sky camera at Mt. Bohyun, Korea (36°N). Journal of Astronomy and Space Sciences 27 (3), 181–188.
Kumar, G.K., Hocking, W.K., 2010. Climatology of northern polar latitude MLT dynamics: mean winds and tides. Annales Geophysicae 28, 1859–1876.
Liu, X., Xu, J., Liu, H.-L., Ma, R., 2008. Nonlinear interactions between gravity waves with different wavelengths and diurnal tide. Journal of Geophysical Research 113 (D8), http://dx.doi.org/10.1029/2007JD009136.
Mayr, H.G., Mengel, J.G., Talaat, E.R., Porter, H.S., Chan, K.L., 2005a. Mesospheric non-migrating tides generated with planetary waves: I. Characteristics. Journal of Atmospheric and Solar-Terrestrial Physics 67 (11), 959–980.
Mayr, H.G., Mengel, J.G., Talaat, E.R., Porter, H.S., Chan, K.L., 2005b. Mesospheric non-migrating tides generated with planetary waves: II. Influence of gravity waves. Journal of Atmospheric and Solar-Terrestrial Physics 67 (11), 981–991.
Mitchell, N.J., Pancheva, D., Middleton, H.R., Hagan, M.E., 2002. Mean winds and tides in the Arctic mesosphere and lower thermosphere. Journal of Geophysical Research 107 (A1), http://dx.doi.org/10.1029/2001JA900127.
Mitchell, N.J., Beldon, C.L., 2009. Gravity waves in the mesopause Region observed by meteor radar: 1. A simple measurement technique. Journal of Atmospheric and Solar-Terrestrial Physics 71 (8–9), 866–874.
Placke, M., Stober, G., Jacobi, C., 2010. Gravity wave momentum fluxes in the MLT—Part I: seasonal variation at Collm (51.31°N, 13.01°E). Journal of Atmospheric and Solar-Terrestrial Physics 73 (9), 904–910.
Sandford, D.J., Beldon, C.L., Hibbins, R.E., Mitchell, N.J., 2010. Dynamics of the Antarctic and Arctic mesosphere and lower thermosphere—Part 1: mean winds. Atmospheric Chemistry and Physics 10 (22), 10273–10289.
Shepherd, T.G., 2000. The middle atmosphere. Journal of Atmosphere and Solar-Terrestrial Physics 62 (17–18), 1587–1601.
Smith, Anne K., 2004. Physics and chemistry of the mesopause region. Journal of Atmospheric and Solar-Terrestrial Physics 66 (10), 839–857.
Taylor, M.J., Ryan, E.H., Tuan, T.F., Edwards, R., 1993. Evidence of preferential directions for gravity wave propagation due to wind filtering in the middle atmosphere. Journal of Geophysical Research 98 (A4), 6047–6057.
Vincent, R.A., Fritts, D.C., 1987. A climatology of gravity wave motions in the mesopause region at Adelaide, Australia. Journal of the Atmospheric Science 44 (4), 748–760.
Vincent, R.A., Hertzog, A., Boccara, G., Vial, F., 2007. Quasi-Lagrangian superpressure balloon measurements of gravity-wave momentum fluxes in the polar stratosphere of both hemispheres. Geophysical Research Letters 34 (19), http://dx.doi.org/10.1029/2007GL031072.
Whiteway, J.A., Duck, T.J., Donovan, D.P., Bird, J.C., Pal, S.R., Carswell, A.I., 1997. Measurements of gravity wave activity within and around the Arctic stratospheric vortex. Geophysical Research Letters 24 (11), 1387–1390.
Wu, D.L., Waters, J.W., 1996. Satellite observations of atmospheric variances: a possible indication of gravity waves. Geophysical Research Letters 23 (24), 3631–3634.
Wu, D.L., Jiang, J.H., 2002. MLS observations of atmospheric gravity waves over Antarctica. Journal of Geophysical Research 107 (D24), http://dx.doi.org/10.1029/2002JD002390.
Wu, D.L., Eckermann, S.D., 2008. Global gravity wave variances from Aura MLS: characteristics and interpretation. Journal of the Atmospheric Sciences 65, 3695–3718.
Yoshiki, M., Kizu, N., Sato, K., 2004. Energy enhancements of gravity waves in the Antarctic lower stratosphere associated with variations in the polar vortex and tropospheric disturbances. Journal of Geophysical Research 109 (D23), http://dx.doi.org/10.1029/2004JD004870.